Journal of Biomedical Optics

BiomedicalOptics.SPIEDigitalLibrary.org

Using infrared and Raman microspectroscopies to compare *ex vivo* involved psoriatic skin with normal human skin

Marie Leroy
Thierry Lefèvre
Roxane Pouliot
Michèle Auger
Gaétan Laroche

SPIE.

Using infrared and Raman microspectroscopies to compare *ex vivo* involved psoriatic skin with normal human skin

Marie Leroy,[a,b,c,d] Thierry Lefèvre,[d] Roxane Pouliot,[c] Michèle Auger,[d] and Gaétan Laroche[a,b,*]
[a]Université Laval, Département de Génie des Mines, de la Métallurgie et des Matériaux, Laboratoire d'Ingénierie de Surface, Centre de Recherche sur les Matériaux Avancés, 1065 Avenue de la médecine, Québec G1V 0A6, Canada
[b]Centre de Recherche du Centre Hospitalier Universitaire de Québec, Hôpital St-François d'Assise, 10 rue de l'Espinay, Québec G1L 3L5, Canada
[c]Centre LOEX de l'Université Laval, Génie Tissulaire et Régénération, LOEX-CRCHU de Québec, Hôpital de l'Enfant Jésus, 1401, 18e rue, Québec G1J 1Z4, Canada
[d]Université Laval, Département de Chimie, Regroupement québécois sur la fonction, la structure et l'ingénierie des protéines, Centre de Recherche sur les Matériaux Avancés, 1045 Avenue de la médecine, Québec G1V 0A6, Canada

Abstract. Psoriasis is a chronic dermatosis that affects around 3% of the world's population. The etiology of this autoimmune pathology is not completely understood. The barrier function of psoriatic skin is known to be strongly altered, but the structural modifications at the origin of this dysfunction are not clear. To develop strategies to reduce symptoms of psoriasis or adequate substitutes for modeling, a deep understanding of the organization of psoriatic skin at a molecular level is required. Infrared and Raman microspectroscopies have been used to obtain direct molecular-level information on psoriatic and healthy human skin biopsies. From the intensities and positions of specific vibrational bands, the lipid and protein distribution and the lipid order have been mapped in the different layers of the skin. Results showed a similar distribution of lipids and collagen for normal and psoriatic human skin. However, psoriatic skin is characterized by heterogeneity in lipid/protein composition at the micrometer scale, a reduction in the definition of skin layer boundaries and a decrease in lipid chain order in the stratum corneum as compared to normal skin. A global decrease of the structural organization is exhibited in psoriatic skin that is compatible with an alteration of its barrier properties. [DOI: 10.1117/1.JBO.20.6.067004]

Keywords: infrared microspectroscopy; Raman microspectroscopy; human skin; psoriasis, lipid organization.

Paper 140843RRR received Dec. 17, 2014; accepted for publication May 11, 2015; published online Jun. 17, 2015.

1 Introduction

Psoriasis is a chronic dermatosis which affects approximately 3% of the world's population. It is an autoimmune and noncontagious pathology which affects both men and women, whatever their age. Unfortunately, the etiology of this autoimmune pathology is still incomplete, even if it is well-documented that psoriasis is modulated by genetic, immunologic, and environmental factors. Psoriatic plaques are characterized by hyperproliferation of keratinocytes (parakeratosis), which leads to failure in the normal differentiation process throughout the living epidermis (LE), and then a disorganization of the skin. The thickening of the viable cell layers (acanthosis), the thickening of the stratum corneum (SC, hyperkeratosis), and the thinning of the epidermis on the top of the dermal papillae, are other histological characteristics of psoriasis plaques.[1–4]

Skin consists of three principal layers: hypodermis, dermis, and epidermis. The skin has a barrier function between the organism and the environment, thanks to the SC, the outermost layer of the skin.[5] In fact, the SC has a well-organized architecture called "bricks and mortar" structure, where the cells (bricks) are embedded in a lipid matrix (mortar). Lipids present in the SC are essentially fatty acids, ceramides, and cholesterol in an equimolar ratio.[5–7] The molecular organization provided by the tightly packed lipid bilayers[6,8] ensures an efficient barrier role.[9] Moreover, the final steps in keratinocyte differentiation are associated with profound changes in their structure, resulting in their transformation into flat and anucleated corneocytes which are interconnected, thanks to intercellular protein structures called corneodesmosomes, which are important for the SC cohesion. Corneocytes are loaded with keratin filaments aligned into a highly organized macrofibrillar matrix and surrounded by a cornified cell envelope. The cornified cell envelope consists of a cross-linked protein envelope which contributes to the biomechanical properties of the cell envelope, and a covalently bound lipid envelope which provides a hydrophobic interface between the hydrophilic surface of the cornified envelope itself and the highly hydrophobic lipid lamellae.[5,10]

In psoriasis, the barrier function of the skin is affected, causing an increase in the transepidermal water loss (TEWL). For instance, Motta et al.[11] showed statistically significant differences between the TEWL of psoriatic plaques and controls. In addition, it has also been shown that the perturbation of the barrier was more important in the most severe psoriatic phenotypes than in chronic plaque psoriasis.[12] Total ceramides in

*Address all correspondence to: Gaétan Laroche, E-mail: gaetan.laroche@gmn.ulaval.ca

1083-3668/2015/$25.00

psoriatic plaques and in normal SC range from 75% to 80% of the total polar lipids as quantified by densitometry. Motta et al.[11,13] showed that the contents of some ceramides were decreased whereas others were increased compared to controls in all types of psoriatic plaques. Among these less abundant ceramides, CER 1 has been suggested to be critical for lamellar bilayer formation in the SC, and hence, for the maintenance of the barrier function. In addition, by comparing psoriatic skin with control samples, Motta et al.[14] found that psoriatic samples presented a higher overall ratio of ceramides and cholesterol with a lower proportion of free fatty acids.

At a structural level, Van Smeden et al.[15] have recently analyzed the lamellar lipid organization of SC isolated from lesional and nonlesional psoriatic skin. These studies exhibit no difference in the lamellar lipid organization between nonlesional psoriatic SC and control SC. On the contrary, a shorter repeat distance of the lamellar lipid phases has been observed in the SC of lesional skin, highlighting a dramatic change in the lipid organization. These changes have been partly attributed to a variation in the amounts of CER 1, in agreement with the studies of Motta et al.,[11,13] but also to a decrease of the lipid chain length that may contribute to a modification in the lipid assembly. The fact that the lipid organization alterations mostly occur on lesional sites implies that factors like inflammation or modifications in the differentiation process play a role in the SC lipid properties of psoriatic skin.[15]

Despite these studies, there is a lack of data regarding the lipid and protein organization in the skin of psoriasis patients. To develop strategies intended to reduce symptoms of psoriasis or adequate substitutes for modeling, a deep understanding of the organization of psoriatic skin at a molecular level is required. Vibrational spectroscopies [infrared (IR) and Raman] are noninvasive and nondestructive optical techniques that can both provide direct molecular-level information on biological tissues. They do not require any special sample preparation or pretreatment. These analytical methods are based on the detection of the frequencies, shapes, and intensities of vibrations of chemical groups that are in turn, sensitive to molecule structure, conformation, and interaction. Accordingly, both IR and Raman spectroscopies have been previously demonstrated to be powerful complementary techniques for the determination of lipid organization and protein secondary structure.[9,16–25]

In IR spectroscopy, stretching modes of the lipid methylene groups are sensitive to the acyl chain conformational order while the amide I band provides information about the overall protein secondary structure.[23] Moreover, sampling with a microscope/multichannel detector coupled to an IR spectrometer allows recording spectra with a spatial resolution of 25 μm^2, thus allowing getting firsthand visual information on sample composition and molecular organization. In addition to providing information on lipid organization (CH_2 stretching modes) and protein structure (amide I and amide II modes), Raman spectroscopy also allows one to obtain specific information about the lipid chain skeletal order from the C—C stretching modes.[18,26–30] Moreover, Raman spectroscopy is particularly sensitive to various amino acid side-chain vibrations. When coupled with a confocal microscope, Raman spectroscopy also allows recording spectra with a spatial resolution on the order of $\sim 1\ \mu m^2$.

In previous studies in which human skin substitutes, made through a self-assembly method, were characterized for the first time using IR and Raman microspectroscopies, we used normal human skin (NHS) as a control and obtained information on its molecular structure and organization. Basically, it was shown that the lipid acyl chains were more ordered in the SC than in other layers.[31] These data were corroborated by Raman microspectroscopy from the so-called C—C stretching mode peak ratios that indicated a decrease in lipid order from the SC to the LE.[32] Based on this characterization of healthy human skin, the objective of the present study is to take advantage of using attenuated total reflectance (ATR)-IR along with IR and Raman microspectroscopies to characterize the molecular organization of psoriatic skin, especially the SC. The results are expected to provide structural clues to explain variations in the barrier function of normal and psoriatic human skins (PHSs).

2 Materials and Methods

2.1 *Patients*

This study was conducted in agreement with the Helsinki declaration and performed under the guidelines of the research ethics committee of the "Centre de Recherche du Centre Hospitalier Universitaire de Québec." All patients were given adequate information to provide written consent. Pathologic samples came from *ex vivo* psoriatic plaques from three patients deceased from heart attack or respiratory failure (thereafter identified as PHSI, PHSII, and PHSIII; 56 yr-old male, 48 yr-old female, and 73 yr-old female, respectively). Normal samples came from several women's breast reduction surgeries (thereafter identified as NHSI, NHSII, NHSIII, NHSIV, and NHSV; 37, 46, 39, 44, and 48 yr-old females, respectively). The information about the patients is summarized in Table 1. Biopsies were cut in small pieces and then embedded in an optimum cutting temperature compound (Tissue-Tek* O.C.T. Compound, Sakura* Finetek) and frozen for further analysis.

2.2 *Histological Analyses*

Five-micrometer-thick cryosections were cut and stained using Masson's Trichrome. The staining allowed distinguishing the different layers of the samples (SC, LE, and dermis).

2.3 *ATR-IR analyses*

IR spectra of the SC of full-thickness skin samples were obtained using a golden gate single reflection ATR system (Specac,

Table 1 Information about the patients.

Skin sample	Sex (age)	Source	Body site
PHSI	M(56)	Deceased patient	Right leg
PHSII	F(48)	Deceased patient	Lower leg
PHSIII	F(73)	Deceased patient	Unknown
NHSI	F(37)	Surgery	Breast
NHSII	F(46)	Surgery	Breast
NHSIII	F(39)	Surgery	Breast
NHSIV	F(44)	Surgery	Breast
NHSV	F(48)	Surgery	Breast

Table 2 Use of the samples.

Skin sample	Experiment
PHSI	Three full-thickness biopsies ATR-IR
	Three sections in microIR
	Three sections in microRaman
PHSII	Three full-thickness biopsies ATR-IR
	Three sections in microIR
	Three sections in microRaman
PHSIII	Three full-thickness biopsies ATR-IR
	Three sections in microIR
	Three sections in microRaman
NHSI	One section in microIR
NHSII	One section in microIR
NHSIII	One section in microIR
	Three sections in microRaman
NHSIV	Six sections in microRaman
NHSV	Four sections in microRaman

Pleasantville, New York) fitted with a diamond crystal. This method probes the first micrometers of the surface of the sample that is in contact with the ATR crystal. Spectra were recorded with a Nicolet Magna 850 Fourier transform spectrometer (Thermo-Nicolet, Madison, Wisconsin) equipped with a narrow-band mercury–cadmium–telluride detector and a germanium-coated KBr beam splitter. At each temperature, a total of 128 interferograms were acquired, coadded and Fourier transformed using a Happ–Genzel apodization function, to give a spectral resolution of 4 cm^{-1} in the spectral range 4000 to 750 cm^{-1}. All data were processed with Grams 8.0 software (Galactic Industries Corp., Salem, Massachusetts). The spectral region corresponding to the CH_2 stretching vibrations was baseline-corrected using a cubic function, and the peak position was determined using the center of gravity at the top 10% of the bands.

2.4 *Infrared microspectroscopy analyses*

Ten micrometer thick cryosections of the samples were placed on reflective-coated microscope slides (Low-e MirrIR, Kevley Technologies, Chesterland, Ohio). IR microscopy images were recorded using an Agilent 620 IR microscope equipped with a liquid-nitrogen cooled 32×32 focal plane array detector and a motorized stage. Each of these 1024 detector elements measured 5.5 $\mu m \times 5.5$ μm, which corresponds to the pixel size in the IR images. This microscope assembly was attached to an Agilent 660 spectrometer. Images were recorded by stacking individual 1024 pixel images recorded by the displacement of the microscope motorized stage. All images were acquired in reflectance mode with each spectrum originating from a detector element being recorded at a 4 cm^{-1} spectral resolution and a 4000 to 1000 cm^{-1} spectral range. For each detector element, 128 interferograms were typically coadded, Fourier transformed, and ratioed over a background recorded from a blank region of the slide. All images were computed using Resolutions Pro software (version 5.2.0.846) while spectra were analyzed using Grams 9.1 (Thermo Fisher, Waltham, Massachusetts). All spectra are presented without any normalization procedure. The region of the spectra between 3150 and 2750 cm^{-1} was baseline corrected using a cubic function.

2.5 *Raman Microspectroscopy Analyses*

The cryotomed transverse 20 μm-thick sections of the samples were put on glass microscope slides. All sections were then analyzed without any further modification.

Raman spectra were recorded using a LabRam HR-800 spectrometer (Horiba Jobin-Yvon, Villeneuve d'Ascq, France) coupled to an Olympus BX-30 fixed stage microscope, equipped with an open electrode Peltier-cooled CCD detector (1024×256 pixels) (Andor Technology, Belfast, Northern Ireland). An MPlan 100× objective (0.90 NA) (Olympus) and an internal He–Ne laser emitting at 633 nm (4-μm^2 illumination spot) were used for the data collection. The confocal hole and the entrance slit of the monochromator (600 lines/mm grating) were fixed at 400 and 100 μm, respectively. All spectra were the result of three acquisitions of 60 s each. Spectra were recorded for two wavelength windows that are 700 to 1800 cm^{-1} (fingerprint region) and 2500 to 3200 cm^{-1} (high-frequency region).

Ten spectra were recorded in each characteristic layer of the samples (SC, LE, and dermis) and were analyzed using GRAMS/AI 8.0 (Thermo Galactic, Salem, New Hampshire). A cubic function was used on each spectral region for the baseline correction to get rid of the fluorescence background.

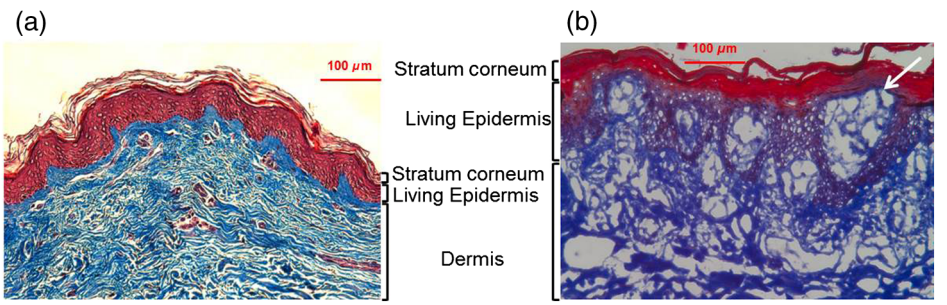

Fig. 1 Histology images of: (a) normal human skin (NHSI) and (b) psoriatic human skin (PHSI) (scale bar = 100 μm)

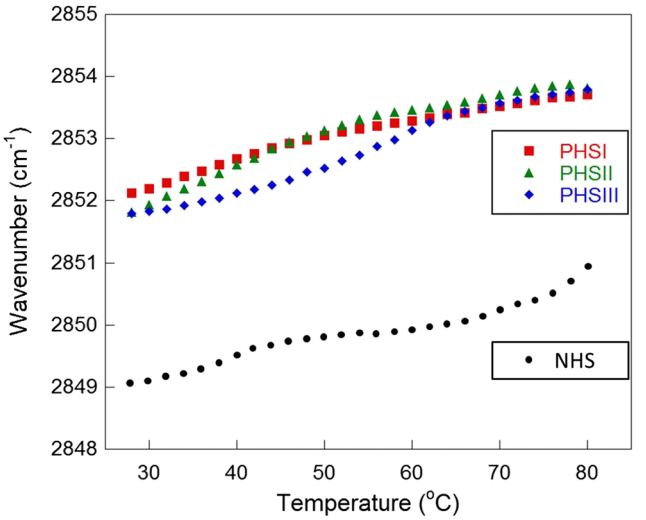

Fig. 2 Thermotropism curves of the stratum corneum of the three PHS samples (I; squares, II; triangles, III; diamonds) compared to NHS control (circles; after[34]).

All spectra were normalized according to different criteria as a function of the spectral feature of interest: in the fingerprint region, spectra were normalized with respect to the amide I band (1650 cm^{-1}) intensity while in the high-frequency region, spectra were normalized using the intensity of the band located at 2930 cm^{-1}.

2.6 *Sample Variability*

For a given psoriatic sample (PHSI, PHSII, and PHSIII), three sections per sample (three sections for PHSI, three sections for PHSII, and three sections for PHSIII) were analyzed in IR and Raman microspectroscopies. For a given normal skin sample, in IR microspectroscopy, one section per sample was analyzed (NHSI, NHSII, and NHSIII); in Raman microspectroscopy, three or more sections per sample were analyzed (three sections for patient NHSIII, five sections for patient NHSIV, and four sections for patient NHSV). Information about the use of the samples is summarized in Table 2. The sections were not taken consecutively, but rather with a random distance between them (between 10 and 100 μm). Despite the natural variability observed in the molecular structure and composition that occurs in biological samples, our data (not shown) demonstrate that the trends in IR and Raman spectra of NHS are similar throughout all investigated samples in terms of peak occurrence, position and shape. By contrast, PHS samples lead to various types of spectra from sample to sample, thus exhibiting less clear general trends. This spectral disparity most likely arises due to the variability in terms of type of psoriasis, medical history of the patient (intake of medicine or topical treatment application), donor site, and so on.

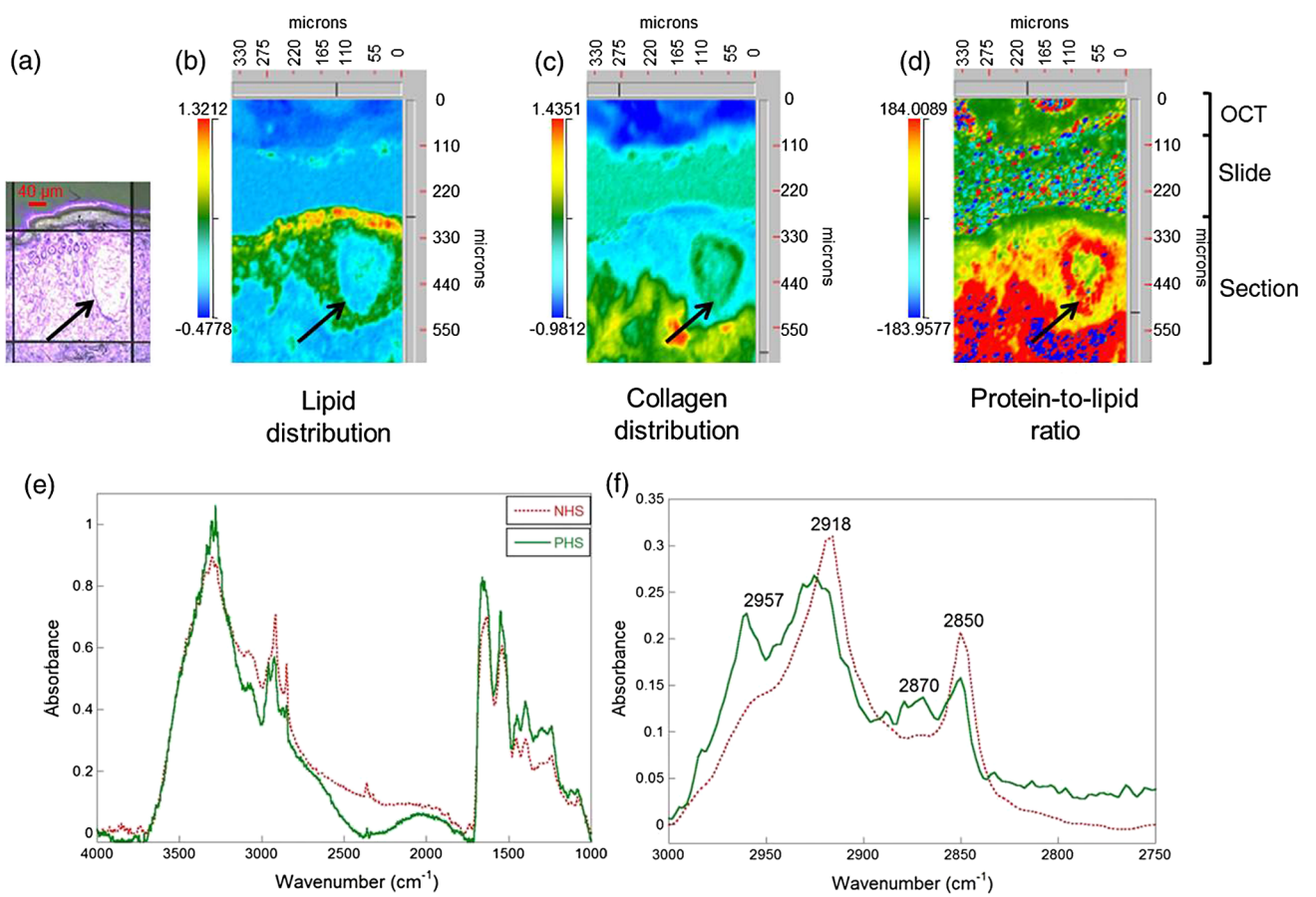

Fig. 3 (a) Microscopic optical view of a PHSI section (15× objective) and corresponding infrared (IR) images showing (b) the lipid distribution, (c) the collagen distribution, and (d) the protein-to-lipid ratio (1 pixel = 5.5 μm). The red dotted line indicates a high content/ratio, whereas the green solid line color indicates a low content/ratio. (e) Superimposition of spectra of the stratum corneum for NHSI and PHSI, and (f) CH_2 stretching mode region.

3 Results and Discussion

3.1 *Histological Analysis*

Figure 1 displays histology images of NHSI and PHSI. The histology image of NHS shows three well defined characteristic layers, i.e., the dermis in blue, the LE in dark red, and the SC in light red. The boundaries between the different layers are sharp and regular and at this scale, the layers seem globally homogeneous. In PHS, it is still possible to distinguish three layers: dermis in blue, LE in purple, and SC in dark red. However, the layer boundaries are somewhat blurred. Moreover, some inclusions seem to be embedded in the LE (an example is evidenced by the white arrow). These inclusions seem to contain some collagen fibers and few cells. According to the literature, these inclusions could be attributed to edema.[33] The overall structure of PHS appears to be less organized than that of NHS.

3.2 *ATR-IR*

The lipid chain order of the SC as a function of temperature measured through ATR-IR spectroscopy is displayed in Figure 2. This figure shows the temperature dependence of the frequency of the CH_2 symmetric stretching mode associated with the lipid chains, measured in the temperature range 28°C to 80°C for both NHS and PHS samples. It is well-known that the position of the band attributed to the symmetric CH_2 stretching mode is sensitive to the lipid chain order. More specifically, it allows distinguishing lipid molecule packing from lipid chain conformational changes. In fact, lipid molecule packing geometry alterations (usually arising from solid–solid phase transitions) are inferred if cooperative changes appear below ~2850 cm^{-1}, while the introduction of *gauche* conformers into the lipid acyl chains appears at higher frequency values.[9] Then higher frequencies of the CH_2 stretching bands are generally characteristic of a high content of *gauche* conformers (disordered state), while bands at lower frequencies are associated with the predominance of *trans* conformers (organized state).

For NHS, a transition is observed between ~35°C and 45°C, and is assigned to a solid–solid (orthorhombic → hexagonal) phase interconversion.[9,24,25] The frequency of the symmetric CH_2 stretching mode then keeps rising with temperature showing that the lipid chains become less ordered. In the case of PHS, the position of the symmetric CH_2 stretching mode is already higher than 2850 cm^{-1} at 28°C, indicating that lipid chains in PHS are in a disordered state near room temperature. The frequency of the symmetric CH_2 stretching mode also increases with temperature, showing that the lipid chains become more disordered. For the whole range of temperatures investigated, the frequency of the CH_2 symmetric stretching mode is always higher than that of the NHS indicating that overall, the lipid chains of the SC of PHS are more disordered than those of the SC of NHS whatever the temperature.

3.3 *Infrared microspectroscopy*

Figure 3 displays (a) optical and IR images of PHSI that were computed to highlight the presence of (b) lipids, (c) collagen,

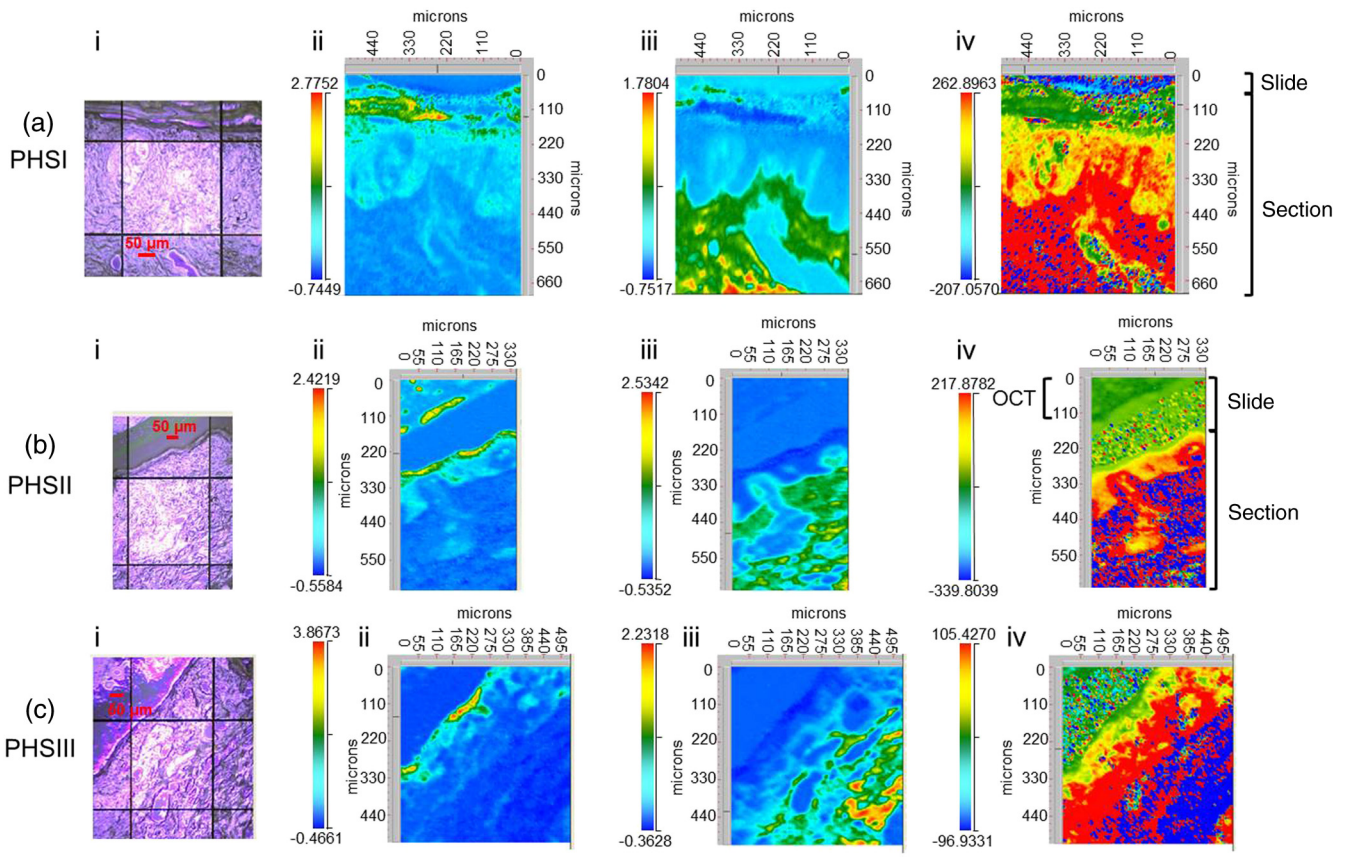

Fig. 4 (i) Microscopic optical views (15× objective) and corresponding IR images showing (ii) the lipid distribution, (iii) the collagen distribution, and (iv) the protein-to-lipid ratio (1 pixel = 5.5 μm) for: (a) PHSI (b) PHSII, and (c) PHSIII.

and (d) lipid-to-protein ratio. Figure 3(b) is generated by representing, on a color scale, the area under the peak centered at ~2850 cm^{-1} (between the two minima surrounding the peak). This image indicates that the lipids are mainly present in the SC. The lipid map distribution also allows distinguishing the LE and the dermis, showing that some lipids are present in the LE whereas they are almost absent in the dermis. The comparison of typical spectra of the SC of PHS and NHS [Figs. 3(e) and 3(f)] further shows that the CH_2 stretching region of NHS is dominated by lipids (bands at 2850 and 2920 cm^{-1}) whereas bands due to proteins are more present for PHS (bands at 2870 and 2950 cm^{-1}). Therefore, the SC of the PHS seems to contain fewer lipids as compared to NHS. This is further confirmed by Fig. 3(b) which displays a poorly defined lipid-rich SC layer with no clear discontinuity with the LE. This is clearly different from the lipid distribution in NHS.[31]

The image generated in Fig. 3(c), computed from the integrated area of the 1342 cm^{-1} feature of collagen (CH_2 and CH_3 wagging and deformation and CN stretching mode), allows localizing collagen in the dermis, thus creating a clear separation between this protein-rich layer on one hand, and the SC and LE on the other hand. In addition, Fig. 3(d) displays the protein-to-lipid content throughout the sample as calculated from the ratio of the integrated area of the amide I peak (centered at 1650 cm^{-1}, between the two minima surrounding the peak) to that of the 2850 cm^{-1} peak. This image shows that the dermis is a protein-rich layer. It is noteworthy that the images of lipids, collagen, and protein-to-lipid ratio distributions are similar for all of the PHS samples (I, II, and III), showing interpenetration between layers. Some of the PHS images (Fig. 4) allowed visualizing the elongation of dermal papillae. By contrast, NHS images display well-separated layers.[31]

The inclusions embedded in the LE of PHS are easily distinguishable in these images [black arrows, Figs. 3(b)–3(d)]. The core of these inclusions contains some lipids (but in fewer amounts with respect to LE) and their periphery is rich in proteins. Since this ring-shaped region seems to be rich in collagen, it is consistent with the fact that the inclusion could be edema. As a matter of fact, edemas are part of the papillar layer of the dermis and can detach and migrate from it.[33] The structure of these inclusions needs to be further investigated.

Figure 5 compares the lipid order maps of NHS and PHS as plotted from the position of the center of gravity of the peak corresponding to the methylene symmetric stretching mode, at approximately 2850 cm^{-1}. Figure 5(b) reveals that the frequency of this mode is significantly lower in the SC relative to the LE for NHS, indicating that the lipid acyl chains are fairly more ordered in the SC layer, in agreement with previously published data.[31] The images obtained from either of the PHS samples [example provided in Fig. 5(d)] do not allow consistent distinguishing of the SC from the LE with a lower definition of the skin layer boundaries in terms of lipid organization.

Focusing on the SC, three random spectra per analyzed sections of PHS samples (I, II, and III) and NHS (I, II, and III) have been taken in the SC. The frequency of the methylene symmetric stretching mode has been measured in each spectrum. The results, summarized in Table 3, clearly evidence that higher frequencies (by about 2 cm^{-1}) are measured in psoriatic samples. This result shows that lipids are less ordered in psoriatic skin, in agreement with the ATR data.

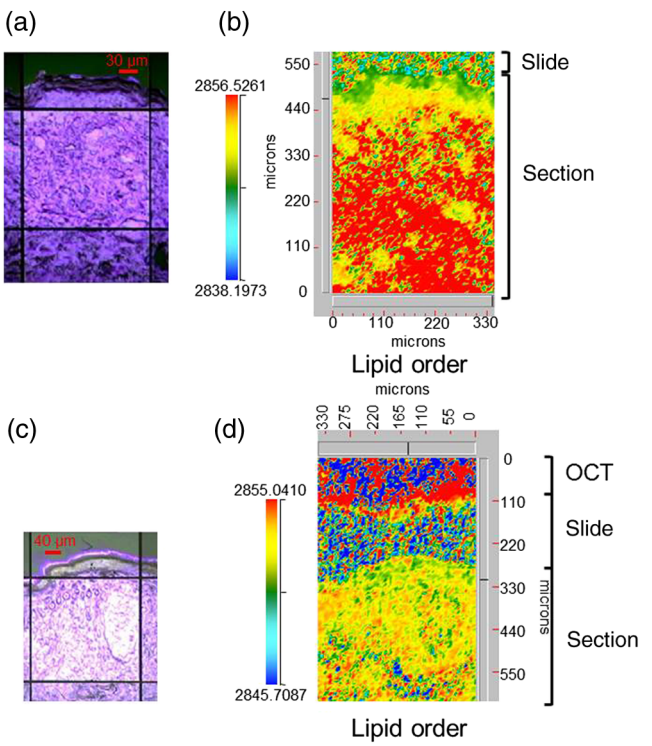

Fig. 5 Microscopic view (15× objective) of: (a) NHSI and (c) PHSI, and the corresponding IR images across skin sections: (b) NHSI and (d) PHSI, computed from the position of the center of gravity of the peak corresponding to the CH_2 symmetric stretching mode [color scale from low (green) to high (red) frequencies].

3.4 *Raman Microspectroscopy*

Further characterization of the lipid distribution and organization was performed using Raman microspectroscopy. Figure 6(a) displays a microscopic view of a section of PHSII. For comparison, a histological image is presented in Fig. 6(b). Red dots in Fig. 6(a) highlight locations where spectra were recorded. In the case of NHS, spectra taken in a given skin layer (either SC, LE or dermis) were similar to each other in terms of peak occurrence and intensities and can be easily coadded to generate an averaged spectrum for this layer. However, in the case of PHS, the spectra recorded from a given layer exhibit several different patterns, showing that the skin is heterogeneous. Spectra had then to be averaged per group of similar spectra. For

Table 3 Average frequency of the peak corresponding to the CH_2 symmetric stretching mode for normal and psoriatic human skin samples.

Samples	Frequency (cm^{-1})	Standard deviation
PHSI	2852.2	0.8
PHSII	2852.6	0.8
PHSIII	2852.6	0.9
NHSI	2850.7	0.6
NHSII	2850.0	0
NHSIII	2850.7	0.5

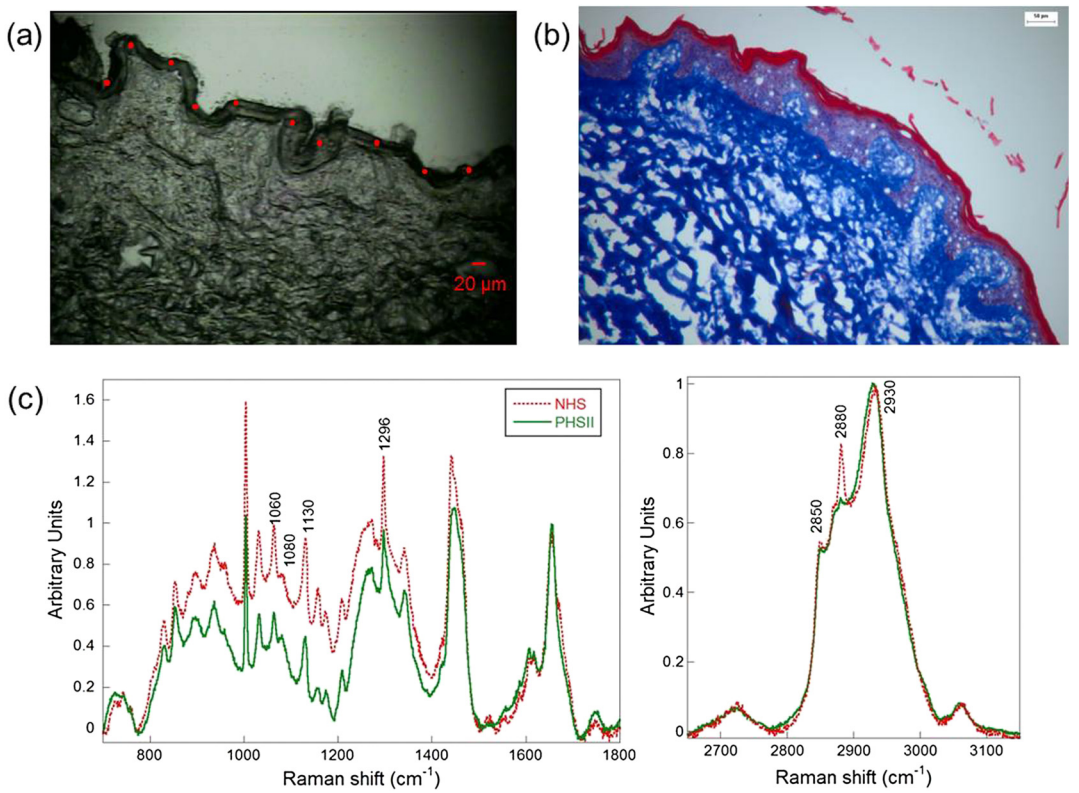

Fig. 6 (a) Optical image of a PHSII section (10× objective). The red dots correspond to the locations where the Raman spectra were recorded prior being averaged (scale bar 20 μm); (b) histological image of a PHSII section (scale bar 100 μm); and (c) Raman spectra of the stratum corneum for NHSIII (see text for details) and PHSII-group 1 in the fingerprint (left) and C—H stretching (right) regions.

instance, some of the spectra recorded from the SC of PHS are similar to those obtained for NHS. Consequently, this series of spectra were averaged and the resulting spectrum is referred as to group 1. However, other spectra of SC of PHS display very similar features to each other, although being significantly different from those of the SC of NHS, and are identified as being part of group 2. Finally, other spectra cannot be grouped together because each of them displays its own spectral profile. These latter spectra will not be discussed any further.

The averaged spectrum from group 1 is shown in Fig. 6(c) as compared with NHS in the fingerprint and high-frequency regions. It exhibits a sharp band at 1296 cm^{-1} (CH_2 twisting mode) which is characteristic of the presence of lipids. However, in the case of PHS, the intensity of this peak is lower and broader than the one of the NHS spectrum [Fig. 6(c)], suggesting that there are fewer lipids in PHS than in NHS. The broadening of this peak further indicates that the lipids are less ordered in PHS. This is confirmed by the CH_2 asymmetric stretching mode at 2880 cm^{-1}, which appears as a shoulder in the case of PHS whereas it is sharp and more intense in the case of NHS. These Raman data overall support the IR observations.

Previous works demonstrated the usefulness of the frequency domain ranging from 1000 to 1150 cm^{-1} to study lipid chain order. Indeed, the vibrational modes at 1060 and 1130 cm^{-1} correspond to the C—C skeletal stretching vibration of lipids in *trans* conformation (ordered phase), whereas the vibrational mode at 1085 cm^{-1} is due to the C—C stretching vibration of lipids in *gauche* conformation (disordered phase).[26] The lipid packing can thus be semiquantitatively evaluated using the I_{1060}/I_{1080} and I_{1130}/I_{1080} intensity ratios.[32] These ratios are presented for both NHS and PHS (from averaged spectra from group 1 of PHSI, PHSII, and PHSIII) in Fig. 7. On average, the values of both ratios are lower in PHS than in NHS, confirming that the lipid chains of the SC are less ordered for PHS than for NHS.

Figure 8(a) displays the superimposition of group 1 and group 2 averaged Raman spectra taken from the SC of a section of PHSIII. As previously mentioned, the red (group 1) spectrum is similar to the averaged spectrum recorded from the SC of NHS in terms of peak occurrence and overall profile. However, the spectrum of group 2 exhibits particular features, such as lower intensities of the bands at 1003 and 1342 cm^{-1} due to proteins (phenylalanine residue and skeletal protein vibrations, respectively[35]) with respect to the lipid band at 1296 cm^{-1}, illustrating that the protein content decreased markedly as compared to lipids.[36] This is further supported by the intensity increase of the peak at 2850 cm^{-1} and the neighboring broad features at ~2900 to 2860 cm^{-1} that are due to CH_2 stretching modes of lipids [Fig. 8(a), inset].

Performing a pixel-by-pixel analysis of the IR images previously recorded further supports the heterogeneous nature of the PHS samples. As a matter of fact, IR spectra recorded from similar locations as Raman spectra from group 1 and group 2 [Fig. 8(a) and 8(b)] also display very distinct features. Again, the typical IR spectrum from group 1 exhibits features resembling those of the SC of NHS while the IR protein and lipid spectral contributions observed in spectra from group 2 behave similarly to what was observed in their Raman counterpart [e.g., decrease of the intensities of the protein amide A at ~3250 cm^{-1}, amide I band at ~1650 cm^{-1}, and amide II band

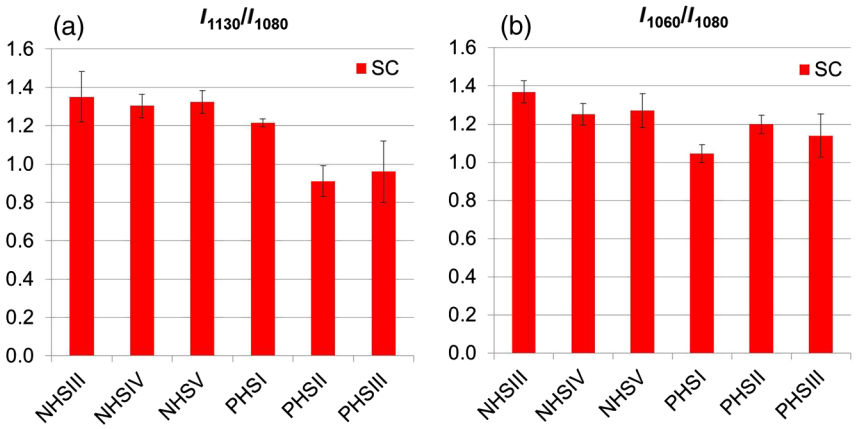

Fig. 7 Histograms of the (a) $I_{1130/1085}$ and (b) $I_{1060/1085}$ ratios for the different specimens.

at ~1550 cm^{-1}, and increase of the absorbance of the lipid spectral contribution at ~2850 cm^{-1} (CH_2 stretching) and ~1744 cm^{-1} (C═O stretching mode)]. It is noteworthy that such spectra did not originate from isolated pixels but were rather observable from several neighboring pixels covering an area of about 500 to 1500 μm^2 (not shown). The SC of PHS thus exhibits significant heterogeneity in lipid/protein composition, some SC regions being characterized by "normal" regions (group 1 spectra) and others by "lipid-rich" regions (group 2 spectra) as shown in Fig. 8(d).

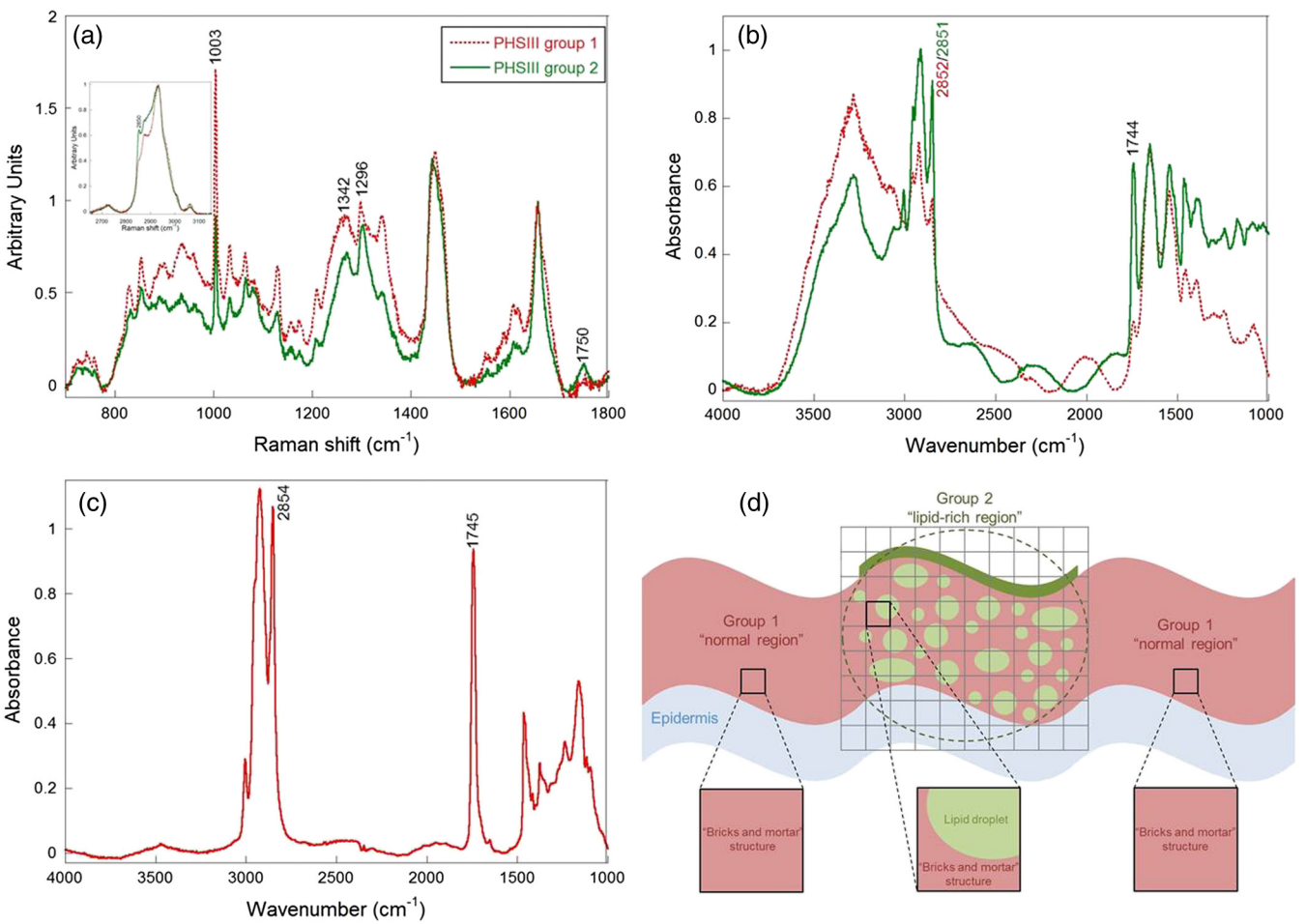

Fig. 8 (a) Superimposition of group 1 and group 2 averaged Raman spectra from the stratum corneum of a single section of PHSIII—the inset shows the C–H stretching region in detail, (b) superimposition of two types of IR spectrum identified in the stratum corneum of a single section of PHSIII, (c) third type of IR spectrum identified in stratum corneum of a single section of PHSIII, and (d) schematic representation of the organization of the stratum corneum of PHSIII (top, the grid represents IR pixels) as deduced from microscopic Raman-IR (bottom, squares represent IR pixels) and optical[12] observations.

Using scanning electron microscopy, Ghadially et al.[12] showed that in chronic psoriasis, the most common type of this skin disease, the number of lipid lamellar bodies appeared normal. Mature lamellar basic unit structures were also of normal dimensions. However, a paucity of intercellular lamellae was observed throughout the intercellular interstices and the mature patterns of lipid bilayers usually observed in the upper SC were not obvious.[12] Last but not least, lipid droplets of about 10 μm and less in diameter were observed in the SC [12]. Considering the spatial resolution of both vibrational techniques that is approx. 4 μm^2 for Raman and 25 μm^2 for IR, the Raman spectra of group 2 and the IR spectra probably correspond to probed areas represented by the overlap of part of these lipids droplets and part of "normal" (protein-rich) SC domains, as represented in Fig. 8(d). The origin of these lipid droplets remains to be elucidated.

As shown in Fig. 8(c), a third type of IR spectra has been recorded. These typical spectra are peculiar in that they are reminiscent of an almost pure lipid region (CH_2 stretching vibrations, C=O stretching mode near 1745 cm^{-1}) with very few proteins (absence of amide bands). Such spectra were observed mainly from an almost continuous layer of about one pixel thick located at the top of the "lipid-rich" domains. This observation is schematized in Fig. 8(d) (dark green thin layer). Solving the origin/attribution of this pure lipid layer requires a deeper investigation.

Only a few studies on skin microspectroscopy were made using human tissues. This work presents the great advantage of bringing information that is of prime interest for pharmacological research, which aims to develop drug formulations adapted to human skin composition and structure. That said, working with human tissues also brings several concerns, most likely due to logistic issues. For instance, the various pathologists who made the biopsies on cadavers did not take care of removing samples of noninvolved skin and consequently, the present study did not allow analyzing with specific internal standards. In addition, scientific research is not the main concern when a human being's death happens. For this reason, cadaver skin samples could take up to one month from the time of death until the analyses. Other issues such as the difficulty of retrieving a sufficient number of samples of human origin to perform appropriate statistical analyses, the different sites where the biopsies were taken, possible contaminations from human sebum, and histology artifacts in the SC area, count among the unpredictable circumstances that may have influenced the interpretation of the data presented herein.

4 Conclusion

IR and Raman microspectroscopies are powerful techniques that allowed characterizing the molecular organization of PHS as compared to that of NHS. Even if the number of PHS samples analyzed in this study is relatively low, several significant observations can be made. More specifically, vibrational microspectroscopies analyses show that the lipids are more ordered in the SC of the NHS than in that of PHS. This lack of order in the lipid chains could explain the deficient barrier function of PHS. Layers of the PHS skin are structurally less defined with respect to NHS, as probed by protein and lipid spectroscopic signatures. Inclusions were detected in the IR images (especially in PHSI), with a protein-rich contour (mainly collagen) and a core essentially containing lipids. The IR images computed from the lipid distribution profile also allowed pointing out that the SC of PHS is poorly defined as opposed to what was observed for NHS. Finally, both Raman and IR spectra recorded from the SC of PHS displayed important differences across this layer, indicating an inhomogeneity in terms of molecular composition that was not evidenced in the SC of NHS.

Acknowledgments

The authors acknowledge the financial support from the Natural Sciences and Engineering Research Council of Canada and the Canadian Institutes for Health Research through their joint Collaborative Health Research program (grant CHRPJ 365395-09), and from the Fonds de recherche du Québec–Nature et technologies (FRQ-NT; grant 2014-PR-173929). The authors also thank Jean-François Rioux-Dubé for his technical support, and Olexandr Bondarenko for helpful discussions on the pathology of skin samples.

References

1. J. E. Gudjonsson and J. T. Elder, "Psoriasis," in *Emery and Rimoin's Essential Medical Genetics*, P. K. Rimoin, Ed, pp. 1–22, Academic Press, London (2013).
2. J. Berth-Jones, "Psoriasis," *Medicine* **41**(6), 334–340 (2013).
3. C. Ryan, A. Menter, and A. M. Bowcock, "Psoriasis," in *Brenner's Encyclopedia of Genetics*, K. Hughes and S. Maloy, Eds., 2nd ed., pp. 524–526, Academic Press, San Diego (2013).
4. M. P. Schon and W. H. Boehncke, "Psoriasis," *N. Engl. J. Med.* **352**(18), 1899–1912 (2005).
5. E. Proksch, J. M. Brandner, and J. M. Jensen, "The skin: an indispensable barrier," *Exp. Dermatol.* **17**(12), 1063–1072 (2008).
6. D. T. Downing, "Lipid and protein structures in the permeability barrier of mammalian epidermis," *J. Lipid Res.* **33**(3), 301–313 (1992).
7. Y. Mizutani et al., "Ceramide biosynthesis in keratinocyte and its role in skin function," *Biochimie* **91**(6), 784–790 (2009).
8. T. Forster, "Cosmetic lipids and the skin barrier," in *Cosmetic Science and Technology*, T. Forster, Ed., Taylor & Francis, New York (2001).
9. R. Mendelsohn, C. R. Flach, and D. J. Moore, "Determination of molecular conformation and permeation in skin via IR spectroscopy, microscopy, and imaging," *Biochim. Biophys. Acta* **1758**(7), 923–933 (2006).
10. C. R. Harding, "The stratum corneum: structure and function in health and disease," *Dermatol. Ther.* **17**(Suppl. 1), 6–15 (2004).
11. S. Motta et al., "Abnormality of water barrier function in psoriasis. Role of ceramide fractions," *Arch. Dermatol.* **130**(4), 452–456 (1994).
12. R. Ghadially, J. T. Reed, and P. M. Elias, "Stratum corneum structure and function correlates with phenotype in psoriasis," *J. Invest. Dermatol.* **107**(4), 558–564 (1996).
13. S. Motta et al., "Ceramide composition of the psoriatic scale," *Biochim. Biophys. Acta* **1182**(2), 147–151 (1993).
14. S. Motta et al., "Content of the different lipid classes in psoriatic scale," *Arch. Dermatol. Res.* **287**(7), 691–694 (1995).
15. J. van Smeden et al., "The important role of stratum corneum lipids for the cutaneous barrier function," *BBA Mol. Cell Biol. Lipids* **1841**(3), 295–313 (2014).
16. X. Zhang et al., "Label-free live-cell imaging of nucleic acids using stimulated Raman scattering microscopy," *Chem. Phys. Chem.* **13**(4), 1054–1059 (2012).
17. Z. Movasaghi, S. Rehman, and I. U. Rehman, "Raman spectroscopy of biological tissues," *Appl. Spectrosc. Rev.* **42**(5), 493–541 (2007).
18. Z. Huang et al., "Evaluation of variations of biomolecular constituents in human skin in vivo by near-infrared Raman spectroscopy," *Biophotonics Instrum. Anal.* **4597**, 109–114 (2001).
19. H. Wang et al., "A method for accurate in vivo micro-Raman spectroscopic measurements under guidance of advanced microscopy imaging," *Sci. Rep.* **3** (2013).
20. G. Jell, R. Swai, and M. M. Stevens, "Raman spectroscopy a tool for tissue engineering," in *Emerging Raman Applications and Techniques in Biomedical and Pharmaceutical Fields*, P. Matousek and M. D. Morris, Eds., pp. 419–437, Springer, Berlin Heidelberg (2010).

21. J. H. Zhao et al., "Real-time raman spectroscopy for noninvasive in vivo skin analysis and diagnosis," in *New Developments in Biomedical Engineering*, D. Campolo, Ed, pp. 455–474, Rijeka, Croatia (2010).
22. G. Zhang et al., "Vibrational microscopy and imaging of skin: from single cells to intact tissue," *Anal. Bioanal. Chem.* **387**(5), 1591–1599 (2007).
23. C. R. Flach and D. J. Moore, "Infrared and Raman imaging spectroscopy of ex vivo skin," *Int. J. Cosmetic Sci.* **35**(2), 125–135 (2013).
24. R. Pouliot et al., "Physical characterization of the stratum corneum of an in vitro human skin equivalent produced by tissue engineering and its comparison with normal human skin by ATR-FTIR spectroscopy and thermal analysis (DSC)," *Biochim. Biophys. Acta* **1439**(3), 341–352 (1999).
25. G. Bernard et al., "Physical characterization of the stratum corneum of an in vitro psoriatic skin model by ATR-FTIR and Raman spectroscopies," *Biochim. Biophys. Acta* **1770**(9), 1317–1323 (2007).
26. A. N. C. Anigbogu et al., "Fourier-transform Raman-spectroscopy of interactions between the penetration enhancer dimethyl sulfoxide and human stratum corneum," *Int. J. Pharm.* **125**(2), 265–282 (1995).
27. P. J. Caspers et al., "In vitro and in vivo Raman spectroscopy of human skin," *Biospectroscopy* **4**(S5), S31–S39 (1998).
28. B. W. Barry, H. G. M. Edwards, and A. C. Williams, "Fourier-transform Raman and infrared vibrational study of human skin-assignment of spectral bands," *J. Raman Spectrosc.* **23**(11), 641–645 (1992).
29. A. Tfayli et al., "Molecular characterization of reconstructed skin model by Raman microspectroscopy: comparison with excised human skin," *Biopolymers* **87**(4), 261–274 (2007).
30. S. M. Ali et al., "Raman spectroscopic analysis of human skin tissue sections ex-vivo: evaluation of the effects of tissue processing and dewaxing," *J. Biomed. Opt.* **18**(6), 061202 (2013).
31. M. Leroy et al., "Characterization of the structure of human skin substitutes by infrared microspectroscopy," *Anal. Bioanal. Chem.* **405**(27), 8709–8718 (2013).
32. M. Leroy et al., "A comparative study between human skin substitutes and normal human skin using Raman microspectroscopy," *Acta Biomater.* **10**(6), 2703–2711 (2014).
33. D. Weedon, "4–the psoriasiform reaction pattern," in *Weedon's Skin Pathology*, D. Weedon, Ed., 3rd ed., pp. 71–91.e18, Churchill Livingstone, Edinburgh (2010).
34. J. Jean et al., "Characterization of a psoriatic skin model produced with involved or uninvolved cells," *J. Tissue Eng. Regen. Med.* (2012).
35. S. Krimm and J. Bandekar, "Vibrational spectroscopy and conformation of peptides, polypeptides, and proteins," in *Advances in Protein Chemistry*, C. B. Anfinsen, J. T. Edsall, and F. M. Richards, Eds, pp. 181–364, Academic Press (1986).
36. H. Wu et al., "In vivo lipidomics using single-cell Raman spectroscopy," *Proc. Natl. Acad. Sci.* **108**(9), 3809–3814 (2011).

Marie Leroy is a chemical engineer who graduated from École Nationale Supérieure de Chimie de Paris in 2009 and received her PhD in 2015 in biomaterials engineering at Université Laval. Her doctoral project focused on using vibrational microspectroscopy to characterize native human skin and human skin substitutes. During her PhD, she contributed to five peer-reviewed publications and was the recipient of several presentation prizes awarded at national and international levels.

Thierry Lefèvre received his PhD in 1997 from the University of Paris 5, followed by a postdoctoral fellowship at the STELA Center at Université Laval. He joined the Department of Chemistry in 2001 as a research associate in Michel Pézolet's group and since 2012 has been in Michèle Auger's group. His research interests regard the molecular structure, interactions, and self-assembly properties of biological molecules using vibrational spectroscopy. This work has been reported in ~45 scientific articles.

Roxane Pouliot joined the Faculty of Pharmacy at Université Laval in 2002 where she was promoted to a full professor in 2011. Her research efforts are focused on the development of a new model of pathologic skin, which is made of cells isolated from patients, biopsies affected with severe skin diseases, such as psoriasis.

Michèle Auger obtained her PhD in 1990 from the University of Ottawa and pursued postdoctoral work at the Massachusetts Institute of Technology. She joined the Department of Chemistry at Université Laval in 1991. Her research efforts are focused on the spectroscopic study of the structure, function, and self-assembly properties of biological molecules. She has published 107 scientific articles and presented 105 invited lectures. The quality of her work has been recognized by several distinctions.

Gaétan Laroche received his PhD in chemistry at Université Laval then went to the Canadian Defence Research and Development Establishment as a postdoctoral trainee. He got professor positions in surgery (1994–2002) and materials engineering (2002–) at Université Laval, where he undertook his research program on biomaterials. He published over 100 publications and presented 75 invited lectures. Recently, he has been awarded the title of Fellow of Biomaterials Science and Engineering for Lifetime Career Achievements.